COMMUNICATION

Interface Control of Ferroelectricity in an $SrRuO_3/BaTiO_3/SrRuO_3$ Capacitor and its Critical Thickness

Yeong Jae Shin, Yoonkoo Kim, Sung-Jin Kang, Ho-Hyun Nahm, Pattukkannu Murugavel, Jeong Rae Kim, Myung Rae Cho, Lingfei Wang, Sang Mo Yang, Jong-Gul Yoon, Jin-Seok Chung, Miyoung Kim, Hua Zhou, Seo Hyoung Chang, and Tae Won Noh**

The atomic-scale synthesis of artificial oxide heterostructures offers new opportunities to create novel states that do not occur in nature. The main challenge related to synthesizing these structures is obtaining atomically sharp interfaces with designed termination sequences. In this study, it is demonstrated that the oxygen pressure (P_{O_2}) during growth plays an important role in controlling the interfacial terminations of $SrRuO_3/BaTiO_3/SrRuO_3$ (SRO/BTO/SRO) ferroelectric (FE) capacitors. The SRO/BTO/SRO heterostructures are grown by a pulsed laser deposition method. The top SRO/BTO interface, grown at high P_{O_2} (around 150 mTorr), usually exhibits a mixture of RuO_2–BaO and SrO–TiO_2 terminations. By reducing P_{O_2}, the authors obtain atomically sharp SRO/BTO top interfaces with uniform SrO–TiO_2 termination. Using capacitor devices with symmetric and uniform interfacial termination, it is demonstrated for the first time that the FE critical thickness can reach the theoretical limit of 3.5 unit cells.

Oxide heterostructures have attracted significant research interest due to the discovery of novel emergent phenomena.[1–11] As a result, heteroepitaxy growth techniques have advanced significantly during the last two decades. However, the task of realizing high quality oxide heterostructures with atomically sharp interfaces is still challenging, even for simple perovskite oxides.[1–12] For instance, it has been widely accepted that each maximum of a reflective high-energy electron diffraction (RHEED) intensity profile during the pulsed laser deposition (PLD) growth corresponds to the growth of one unit cell. The perovskite stacking sequence is therefore expected to be preserved during stoichiometric deposition (i.e., a unit-cell-by-unit-cell growth scheme). However, recent studies have shown that RHEED oscillations alone do not provide sufficient information to confirm the intended atomic structure of the surface.[13–15] During PLD growth, numerous growth variables, including chemical stabilities and mobilities of surface adatoms, can be altered by the growth conditions. This alteration may in turn give rise to uncontrollable changes of surface termination.[14,15] Up to this point, there have been few investigations on how the key growth parameters, e.g., oxygen pressure (P_{O_2}) and temperature, affect surface termination.

Ultrathin ferroelectric (FE) heterostructures are model systems in which physical properties are highly dependent on the interfacial structure. As the FE film thickness decreases, the FE polarization decreases monotonically and finally disappears at a critical thickness. According to theoretical predictions,

Y. J. Shin, Dr. S.-J. Kang, Dr. H.-H. Nahm, J. R. Kim, Dr. M. R. Cho, Dr. L. Wang, Prof. T. W. Noh
Center for Correlated Electron Systems
Institute for Basic Science (IBS)
Seoul 08826, Republic of Korea
E-mail: twnoh@snu.ac.kr

Y. J. Shin, Dr. S.-J. Kang, Dr. H.-H. Nahm, J. R. Kim, Dr. M. R. Cho, Dr. L. Wang, Prof. T. W. Noh
Department of Physics and Astronomy
Seoul National University
Seoul 08826, Republic of Korea

Y. Kim, Prof. M. Kim
Department of Materials Science and Engineering and Research Institute of Advanced Materials
Seoul National University
Seoul 08826, Republic of Korea

Prof. P. Murugavel
Department of Physics
Indian Institute of Technology Madras
Chennai 600036, India

Prof. S. M. Yang
Department of Physics
Sookmyung Women's University
Seoul 04310, Republic of Korea

Prof. J.-G. Yoon
Department of Physics
University of Suwon
Hwaseong, Gyunggi-do 18323, Republic of Korea

Prof. J.-S. Chung
Department of Physics
Soongsil University
Seoul 06978, Republic of Korea

Dr. H. Zhou
Advanced Photon Source
Argonne National Laboratory
Lemont, IL 60439, USA

Prof. S. H. Chang
Department of Physics
Pukyong National University
Busan 48513, Republic of Korea
E-mail: cshyoung@pknu.ac.kr

DOI: 10.1002/adma.201602795

© 2017 WILEY-VCH Verlag GmbH & Co. KGaA, Weinheim

15214095, 2017, 19, Downloaded from https://onlinelibrary.wiley.com/doi/10.1002/adma.201602795 by Chung-Ang University, Wiley Online Library on [12/12/2022]. See the Terms and Conditions (https://onlinelibrary.wiley.com/terms-and-conditions) on Wiley Online Library for rules of use; OA articles are governed by the applicable Creative Commons License

COMMUNICATION

15214095, 2017, 19, Downloaded from https://onlinelibrary.wiley.com/doi/10.1002/adma.201602795 by Chung-Ang University, Wiley Online Library on [12/12/2022]. See the Terms and Conditions (https://onlinelibrary.wiley.com/terms-and-conditions) on Wiley Online Library for rules of use; OA articles are governed by the applicable Creative Commons License

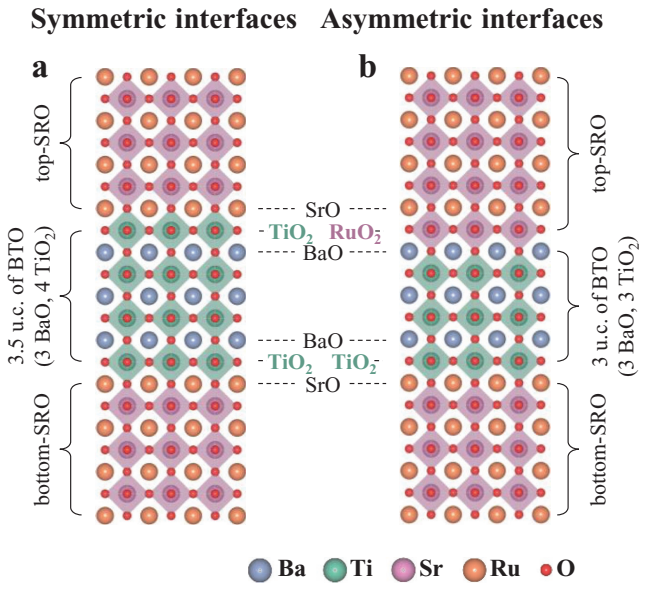

Scheme 1. Schematic of the possible atomic stackings of the $SrRuO_3$/$BaTiO_3$/$SrRuO_3$ (SRO/BTO/SRO) heterostructure with a) symmetric SrO–TiO_2 interfaces, which result in a BTO layer thickness (t_{BTO}) of 3.5 u.c., and with b) BaO–RuO_2 and SrO–TiO_2 interfaces at the top and bottom of the BTO layer, respectively, which result in t_{BTO} = 3 u.c. Note that the asymmetric case (b) occurs under the commonly assumed unit-cell-by-unit-cell growth mode.

the prototypical all-oxide $SrRuO_3$/$BaTiO_3$/$SrRuO_3$ (SRO/BTO/SRO) heterostructure should have a critical thickness between 3.5 and 6.5 unit cells (u.c.).[16,17] However, experimental critical thicknesses are significantly larger. Recent studies on SRO/BTO/SRO capacitors have shown that a lack of atomic scale interface control is the main obstacle to obtaining FE critical thicknesses approaching the theoretical limit.[18,19] The experimental structures feature mixed terminations and the resulting pinned dipoles notably degrade the FE polarization stability, which results in the suppression of ferroelectric behavior below about 20 u.c.[19]

Here, we demonstrate the critical role of P_{O_2} in determining the interface termination. Using scanning transmission electron microscopy (STEM) and X-ray diffraction (XRD), the interfaces of SRO/BTO heterostructures were studied for P_{O_2} = 5 and 150 mTorr. At 150 mTorr, we found a mixed interfacial termination. However, for P_{O_2} = 5 mTorr, a singly terminated interface was observed. Density functional theory (DFT) calculations also support that the stability of the possible interface atomic structures are significantly affected by changing P_{O_2}. Capacitor devices grown at P_{O_2} = 5 mTorr with well-controlled interfaces show FE critical thicknesses as low as 3.5 u.c. in agreement with theory.[16]

The SRO/BTO/SRO capacitor can have two possible atomic arrangements, as illustrated in **Scheme 1**. Since RuO_2 is thermally unstable during high temperature deposition, the bottom SRO layer is always SrO terminated.[15] Therefore, the BTO layer starts with TiO_2. Following the commonly assumed unit-cell-by-unit-cell growth mode, the growth of the BTO layer should end with a top BaO termination. As a result, the top interface should have the sequence BaO–RuO_2, which produces an asymmetric capacitor configuration (Scheme 1b). On the other hand, FE critical thickness calculations have been performed only for ideal symmetric configurations with TiO_2 termination on both top and bottom BTO surfaces (Scheme 1a).[16,17] Obtaining such a symmetric termination configuration is essential to test the theoretically predicted value of the FE critical thickness.

Fully strained SRO/BTO/SRO heterostructures were fabricated using PLD on atomically smooth TiO_2-terminated $SrTiO_3$(001) substrates. The thicknesses of the bottom and top SRO electrodes were fixed at 20 nm. During the BTO growth, P_{O_2} was set to either 5 or 150 mTorr. The t_{BTO} was controlled by monitoring the high pressure RHEED intensity oscillations. In the ideal layer-by-layer growth mode, the number (n) of RHEED oscillations signifies a BTO layer with thickness $t_{BTO} = n$ u.c. However, by using STEM we found that the films grown at P_{O_2} = 5 mTorr end with a half-unit-cell BTO layer (Figure S1, Supporting Information). In this case, we denote the film thickness by $t_{BTO} = (n - 0.5)$ u.c. Using XRD (Figure S2, Supporting Information), we exclude the formation of secondary phases for both growth conditions (P_{O_2} = 150 and 5 mTorr).

For P_{O_2} = 150 mTorr, we found that two types of termination sequence coexist at the top SRO/BTO interface. **Figure 1**a shows a cross-sectional high-angle annular dark field (HAADF) image from STEM, viewed along the [100] zone axis. The HAADF image displays an atomically sharp BTO/SRO bottom interface with the expected TiO_2–SrO termination sequence. By contrast, the SRO/BTO top interface termination is highly inhomogeneous. Figure 1b,c presents the magnified HAADF images for two regions marked in Figure 1a (dashed boxes I and II). The intensity profiles along the B-site cations are also plotted in the right panels. Note that the intensity of the Ti peaks is lower than those of the Ru peaks due to the smaller atomic number. Four (three) TiO_2 layers imply that the BTO film thickness is 3.5 u.c. (3 u.c.), and the resulting SrO–TiO_2 (RuO_2–BaO) interface will produce a symmetric (asymmetric) capacitor configuration. The mixed termination sequence of the top surface was confirmed by STEM images of different regions of the sample (Figure S3, Supporting Information).

In the SRO/BTO/SRO capacitor with mixed interfacial termination, the local FE response varies significantly. Using the electron-beam lithography technique, we fabricated a 5×5 μm^2 square-shaped capacitor (see Experimental Section). We then chose 10×10 grid positions on the SRO top electrode layer and characterized the local FE responses at each grid point by PFM (Figure S4, Supporting Information).[20] As shown in Figure 1d, we can observe two typical piezoresponse signals. In region (i) (left panel), the PFM phase–voltage curve shows a fully saturated hysteresis and the PFM amplitude–voltage curve has a nearly symmetric butterfly shape, indicating robust and switchable ferroelectricity. By contrast, in region (ii) (right panel) the PFM amplitude and phase show FE polarization switching characteristics only for the downward polarization state (pointing towards the bottom SRO). This result implies that FE polarization in region (ii) is strongly pinned along one direction. The existence of pinned dipoles in the mixed terminated SRO/BTO/SRO capacitor was also proposed by earlier works.[18,19,21]

In order to map the spatial variation of the ferroelectricity, we calculated the ratio between the PFM amplitudes at ±6 V

© 2017 WILEY-VCH Verlag GmbH & Co. KGaA, Weinheim

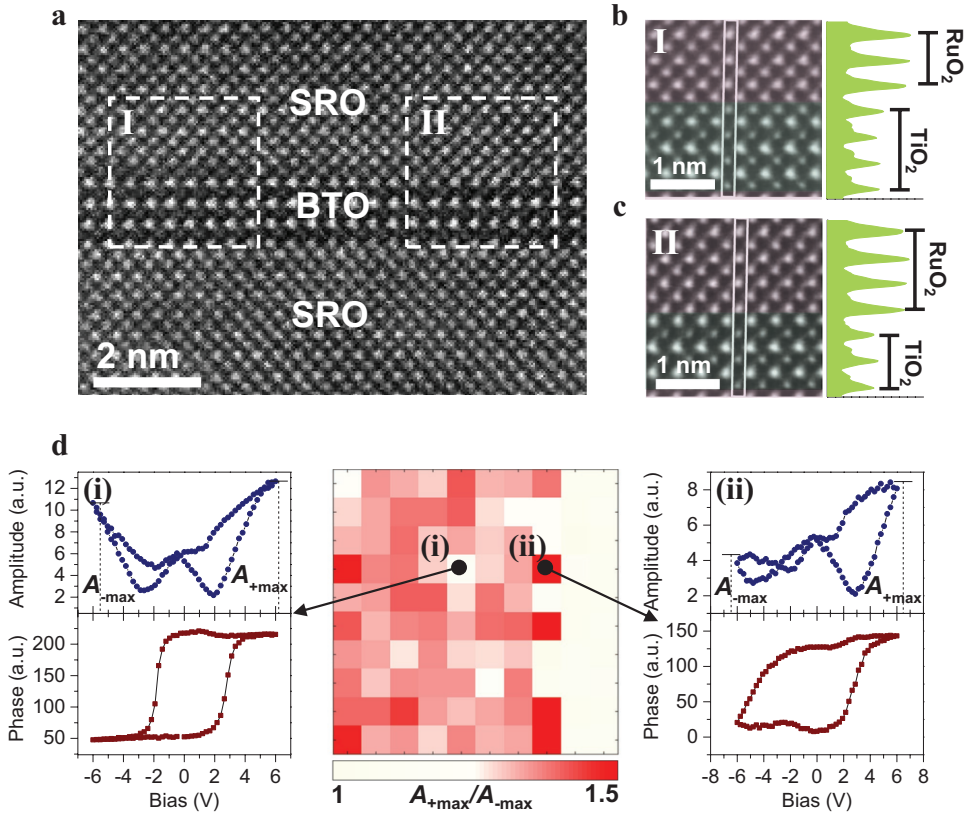

Figure 1. a) STEM image of the SRO/BTO/SRO heterostructure with P_{O_2} equal to 150 mTorr during BTO growth. The magnified STEM images and intensity profiles are marked by the dashed boxes in 1a and show a mixture of b) TiO_2 and c) BaO top terminations of the BTO layer. The t_{BTO} are 3.5 u.c. (3 BaO and 4 TiO_2) and 3 u.c. (3 BaO and 3 TiO_2) for (b) and (c), respectively. d) The amplitude and phase from piezoresponse force microscopy (PFM) hysteresis loops collected in different locations reveal piezoresponse in both polarization directions (left) and highly pinned piezoresponse along the downward polarization direction (right). The color map at the center of 1d displays the ratio of maximum PFM amplitude response (A_{+max}/A_{-max}) at positive bias (A_{+max}) to that at negative bias (A_{-max}). The black dots marked by (i) and (ii) indicate the points where the left and right plots were measured.

(A_{+max}/A_{-max}) at each sampling point. As shown in the central panel of Figure 1d, for ≈50% of points the A_{+max}/A_{-max} ratio is close to 1.0, signifying switchable FE response (region (i)). For the remaining points, A_{+max}/A_{-max} is much higher than 1.0, signifying the response of pinned dipoles (region (ii)). It is therefore difficult to test the FE critical thickness experimentally with the SRO/BTO/SRO capacitors grown at P_{O_2} = 150 mTorr.

In contrast, the heterostructure grown at P_{O_2} = 5 mTorr has a uniform BTO top interface and a symmetric termination sequence (Scheme 1a). As shown in **Figure 2**a,b, the high resolution HAADF images reveal atomically sharp interfaces formed over a lateral range of 40 nm. The BTO layer is uniformly TiO_2-terminated for both the top and bottom interfaces. The intensity profile along the solid box in Figure 2b also confirms the symmetric SrO–TiO_2 interface termination sequences (Figure 2c). In this sample with alternatively stacked three BaO and four TiO_2 layers we denote the t_{BTO} as 3.5 u.c (Figure 2d).

Considering that the STEM images only provide local structural information, we also performed surface X-ray scattering measurements and COBRA to further confirm the uniformity of the BTO interfaces.[22] The sample used for this measurement contains a 5 mTorr grown BTO layer (3.5 u.c.) sandwiched between two SRO layers (3 u.c. each). The COBRA electron density mapping (Figure 2e) indicates that the symmetric SrO–TiO_2 interface termination occurs uniformly over the size of the X-ray beam spot, which is typically 30 μm in diameter. These structural investigations clearly indicate that the heterostructure grown with P_{O_2} = 5 mTorr has a uniformly TiO_2-terminated interface.

We now turn to possible interpretations of the observed P_{O_2}-dependent termination change. We first checked the cation stoichiometry of the BTO films. Some earlier studies showed that different background pressures could change the composition or stoichiometry of BTO during the growth.[23–25] However, STEM-energy dispersive spectroscopy confirms that our films grown at different P_{O_2} are close to stoichiometric with the Ti/Ba ratio very close to one (Figure S5, Supporting information). To check the oxygen stoichiometry, we evaluated the lattice constant of the BTO layer with P_{O_2} = 5 mTorr from the COBRA electron density map. The measured *c*-axis lattice constant was quite consistent with that of a fully strained BTO film on a $SrTiO_3$ (001) substrate. This indicates that there is no significant amount of oxygen vacancies in our BTO layer even with a lower P_{O_2} condition. Therefore, we exclude the possibility that deviations in film stoichiometry play a significant role in affecting the composition of the BTO surface and interface termination.

© 2017 WILEY-VCH Verlag GmbH & Co. KGaA, Weinheim

15214095, 2017, 19, Downloaded from https://onlinelibrary.wiley.com/doi/10.1002/adma.201602795 by Chung-Ang University, Wiley Online Library on [12/12/2022]. See the Terms and Conditions (https://onlinelibrary.wiley.com/terms-and-conditions) on Wiley Online Library for rules of use; OA articles are governed by the applicable Creative Commons License

15214095, 2017, 19, Downloaded from https://onlinelibrary.wiley.com/doi/10.1002/adma.201602795 by Chung-Ang University, Wiley Online Library on [12/12/2022]. See the Terms and Conditions (https://onlinelibrary.wiley.com/terms-and-conditions) on Wiley Online Library for rules of use; OA articles are governed by the applicable Creative Commons License

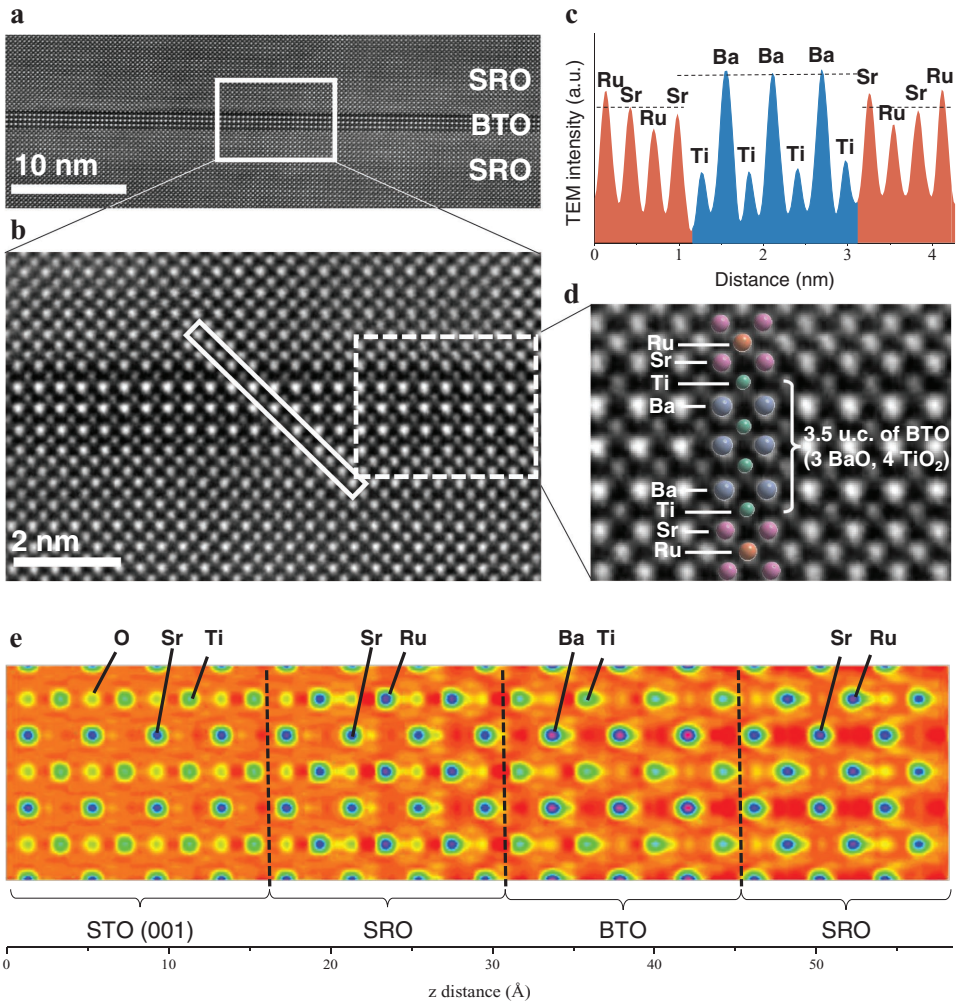

Figure 2. a) STEM image of the SRO/BTO/SRO heterostructure with P_{O_2} = 5 mTorr. b) Magnified STEM image of the region inside the white box in 2a. c) Intensity line profile corresponding to the highlighted solid box in (b). This profile clearly shows the TiO_2 termination at the top and bottom of the BTO layer. d) Magnified image of the area inside the white box in (b). The different atomic species are indicated by colored circles. In the entire measured region, the BTO layer is composed of three BaO layers and four TiO_2 layers, indicating t_{BTO} = 3.5 u.c. e) Coherent Bragg rod analysis (COBRA) electron density for the BTO film grown with P_{O_2} = 5 mTorr. The electron density map shows the (110) plane through Sr, Ba, Ti, Ru, and O. The COBRA maps show that the BTO layer has uniform and sharp interfaces over a large length scale (i.e., at least ≈30 μm).

Another possible interpretation is that the P_{O_2} dependent termination could be related to the stability of BaO and TiO_2 terminations during growth. The stability of each component can play an important factor in determining the interface terminations. A typical example is epitaxial SRO films grown on $SrTiO_3$ (001) substrates. It is already widely known that termination conversion can occur during the growth of epitaxial SRO films.[15,26–28] The highly volatile nature of RuO_2 makes the RuO_2-termination unstable during high-temperature growth, leading to a conversion to SrO-termination. For BTO, the stabilities of possible surface structures were reported to be strongly dependent on the background oxygen pressure.[29,30] A change in relative stability may also act as a driving force for forming different surface terminations of BTO. To investigate this idea, we performed DFT calculations on the Gibbs free energies of BaO- and TiO_2-terminated BTO surfaces (Section VI, Supporting Information). The DFT calculations showed that the TiO_2 termination becomes more stable with decreasing P_{O_2} (Figure S6, Supporting Information). This is qualitatively consistent with our experimental observations. The change of stability may imply a different bonding strength for each termination which may in turn affect the actual kinetic growth process of PLD and ultimately the termination. Nonetheless, the nonequilibrium nature of PLD makes connecting the DFT results with our experiment challenging. Additional factors that could also affect the surface termination include the density of excited arrived species and surface/arrived species interactions. Further study of the exact mechanism that determines the surface termination is therefore required.

Using BTO capacitors with symmetric interfaces, we investigated the FE critical thickness and experimentally confirmed a robust FE response down to t_{BTO} = 3.5 u.c. We performed PFM hysteresis loop measurements at 10 × 10 grid points on a capacitor with 5 × 5 μm² sizes. **Figure 3**a displays the calculated A_{+max}/A_{-max} ratio of PFM loops measured at each grid point for a t_{BTO} = 3.5 u.c. capacitor. The local variation of the FE response

© 2017 WILEY-VCH Verlag GmbH & Co. KGaA, Weinheim

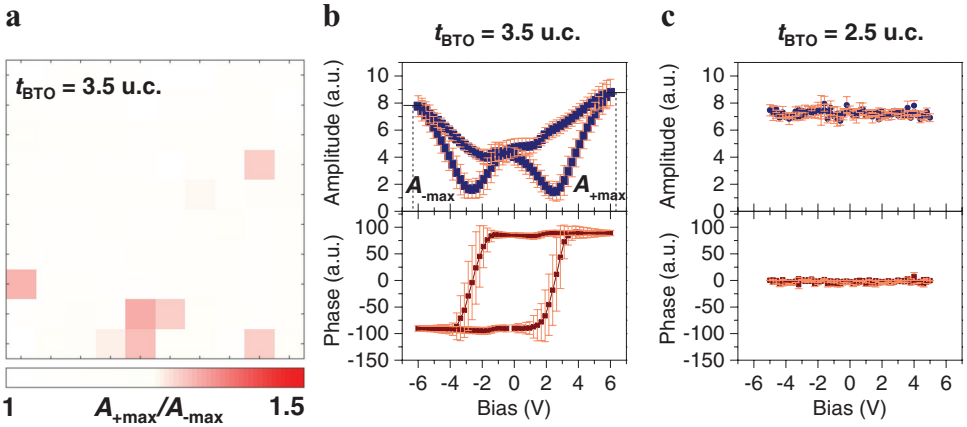

Figure 3. a) Color map of A_{+max}/A_{-max} for the SRO/BTO/SRO capacitor with t_{BTO} = 3.5 u.c. and P_{O_2} = 5 mTorr. b) Averaged PFM amplitude and phase hysteresis loops measured at 10 × 10 different positions in a single capacitor. The error bar indicates the standard deviation of the measured loops. c) Averaged PFM amplitude and phase hysteresis loops of the SRO/BTO/SRO capacitor with t_{BTO} = 2.5 u.c.

is much smaller than in the sample with mixed BTO termination. For the majority of points, the A_{+max}/A_{-max} values are very close to 1.0, indicating symmetric and switchable FE polarization. The averaged PFM hysteresis loops (Figure 3b) also show symmetric butterfly-shaped amplitude–voltage curves and fully saturated phase–voltage curves that are uniform within the error bar. Template matching analysis[31] on the STEM images also shows that the Ti ions are displaced by about 0.1 Å relative to the center position of surrounding Ba ions, further supporting the polar nature of 3.5 u.c. BTO samples (Figure S7, Supporting Information). On the other hand, the FE signatures disappear for BTO capacitors with t_{BTO} = 2.5 u.c. (Figure 3c), meaning the FE critical thickness in our devices is 3.5 u.c. This value is smaller than some theoretical values[17,32] but is consistent with the DFT calculations of G. Gera et al., who included charge distribution effects at the interface beyond the Thomas–Fermi capacitor.[16]

In summary, we investigated the significant effect of background oxygen pressure on SRO/BTO interface termination. We found that symmetric interfaces with uniform TiO_2-terminations are crucial for decreasing ferroelectric critical thickness in SRO/BTO/SRO heterostructures and can only be obtained utilizing a lower oxygen condition (i.e., around P_{O_2} = 5 mTorr). As a result, we succeeded in demonstrating the theoretically predicted critical thickness of 3.5 u.c. in a real FE capacitor.[16] Our results suggest that termination control at the atomic scale will serve as a useful tool for exploring the emergent properties of oxide heterostructures and functional devices.

Experimental Section

Sample Fabrication and Structural Characterization: The SRO/BTO/SRO heterostructures were grown using the PLD technique on $SrTiO_3$ (001) substrates with a miscut angle of less than 0.1°. A KrF excimer laser (248 nm, COMPex pro, Coherent) was used to ablate the SRO or BTO ceramic targets. The deposition temperature was maintained at 700 °C during the entire growth process. BTO epitaxial films were grown under P_{O_2} conditions of 5 and 150 mTorr. SRO top and bottom films were grown under P_{O_2} conditions of 100 mTorr.

The high quality of the films was confirmed using a scanning transmission electron microscope (JEM-ARM200F, JEOL). The structure of the samples was investigated by surface X-ray scattering measurements and COBRA performed using Huber six-circle diffractometers at Sector 12ID-D of the advanced photon source and at Sector 9C of the Pohang light source. For the electrical measurements of the BTO layer, capacitor devices with diameters from 500 nm to 10 µm were fabricated using e-beam lithography and ion milling.

PFM Measurements: The ferroelectric polarization switching properties were measured using an atomic force microscopy system (Cypher Asylum) at room temperature. A commercially available Cr/Pt-coated probe tip with a spring constant of ≈40 N m^{-1} and a resonant frequency of ≈400 kHz (Tap300E, Budget Sensors) was used. The contact resonance frequency was 1.2–1.3 MHz. The high spring constant and contact resonance frequency minimized possible effects of nonpiezoelectric response, such as electrostatic force.[33,34]

Supporting Information

Supporting Information is available from the Wiley Online Library or from the author.

Acknowledgements

This work was supported by IBS-R009-D1 through the Research Center Program of the Institute for Basic Science in Korea. S.H.C. was supported by Basic Science Research Programs through the National Research Foundation of Korea (NRF-2015R1C1A1A01053163). Use of Advanced Photon Source was supported by the U.S. Department of Energy, Office of Science, Office of Basic Energy Sciences, under Contract No. DE-AC02-06CH11357. STEM analysis was supported by the National Center for Inter-University Research Facilities (NCIRF) in Seoul National University in Korea.

Received: May 26, 2016
Revised: December 21, 2016
Published online: March 3, 2017

[1] H. Y. Hwang, Y. Iwasa, M. Kawasaki, B. Keimer, N. Nagaosa, Y. Tokura, *Nat. Mater.* **2012**, *11*, 103.
[2] J. Heber, *Nature* **2009**, *459*, 28.
[3] J. Mannhart, D. G. Schlom, *Science* **2010**, *327*, 1607.
[4] P. Zubko, S. Gariglio, M. Gabay, P. Ghosez, J.-M. Triscone, *Annu. Rev. Condens. Matter Phys.* **2011**, *2*, 141.
[5] J. Chakhalian, A. J. Millis, J. Rondinelli, *Nat. Mater.* **2012**, *11*, 92.

© 2017 WILEY-VCH Verlag GmbH & Co. KGaA, Weinheim

15214095, 2017, 19, Downloaded from https://onlinelibrary.wiley.com/doi/10.1002/adma.201602795 by Chung-Ang University, Wiley Online Library on [12/12/2022]. See the Terms and Conditions (https://onlinelibrary.wiley.com/terms-and-conditions) on Wiley Online Library for rules of use; OA articles are governed by the applicable Creative Commons License

15214095, 2017, 19, Downloaded from https://onlinelibrary.wiley.com/doi/10.1002/adma.201602795 by Chung-Ang University, Wiley Online Library on [12/12/2022]. See the Terms and Conditions (https://onlinelibrary.wiley.com/terms-and-conditions) on Wiley Online Library for rules of use; OA articles are governed by the applicable Creative Commons License

[6] A. Ohtomo, H. Y. Hwang, *Nature* **2004**, *427*, 423.
[7] M. Huijben, A. Brinkman, G. Koster, G. Rijnders, H. Hilgenkamp, D. H. A. Blank, *Adv. Mater.* **2009**, *21*, 1665.
[8] H. Chen, A. M. Kolpak, S. Ismail-Beigi, *Adv. Mater.* **2010**, *22*, 2881.
[9] N. Reyren, S. Thiel, A. D. Caviglia, L. F. Kourkoutis, G. Hammerl, C. Richter, C. W. Schneider, T. Kopp, A.-S. Ruetschi, D. Jaccard, M. Gabay, D. A. Muller, J.-M. Triscone, J. Mannhart, *Science* **2007**, *317*, 1196.
[10] Y. Kozuka, M. Kim, C. Bell, B. G. Kim, Y. Hikita, H. Y. Hwang, *Nature* **2009**, *462*, 487.
[11] A. K. Yadav, C. T. Nelson, S. L. Hsu, Z. Hong, J. D. Clarkson, C. M. Schlepütz, A. R. Damodaran, P. Shafer, E. Arenholz, L. R. Dedon, D. Chen, A. Vishwanath, A. M. Minor, L. Q. Chen, J. F. Scott, L. W. Martin, R. Ramesh, *Nature* **2016**, *530*, 198.
[12] N. Nakagawa, H. Y. Hwang, D. A. Muller, *Nat. Mater.* **2006**, *5*, 204.
[13] J. Shin, A. Y. Borisevich, V. Meunier, J. Zhou, E. W. Plummer, S. V Kalinin, A. P. Baddorf, *ACS Nano* **2010**, *4*, 4190.
[14] A. Tselev, R. K. Vasudevan, A. G. Gianfrancesco, L. Qiao, P. Ganesh, T. L. Meyer, H. N. Lee, M. D. Biegalski, A. P. Baddorf, S. V Kalinin, *ACS Nano* **2015**, *9*, 4316.
[15] G. Rijnders, D. H. A. Blank, J. Choi, C.-B. Eom, *Appl. Phys. Lett.* **2004**, *84*, 505.
[16] G. Gerra, A. K. Tagantsev, N. Setter, K. Parlinski, *Phys. Rev. Lett.* **2006**, *96*, 107603.
[17] J. Junquera, P. Ghosez, *Nature* **2003**, *422*, 506.
[18] X. Liu, Y. Wang, P. V. Lukashev, J. D. Burton, E. Y. Tsymbal, *Phys. Rev. B* **2012**, *85*, 125407.
[19] H. Lu, X. Liu, J. D. Burton, C. W. Bark, Y. Wang, Y. Zhang, D. J. Kim, A. Stamm, P. Lukashev, D. A. Felker, C. M. Folkman, P. Gao, M. S. Rzchowski, X. Q. Pan, C. B. Eom, E. Y. Tsymbal, A. Gruverman, *Adv. Mater.* **2012**, *24*, 1209.
[20] S. Jesse, A. P. Baddorf, S. V. Kalinin, *Appl. Phys. Lett.* **2006**, *88*, 21.
[21] G. Gerra, A. K. Tagantsev, N. Setter, *Phys. Rev. Lett.* **2007**, *98*, 207601.
[22] H. Zhou, Y. Yacoby, V. Y. Butko, G. Logvenov, I. Bozovic, R. Pindak, *Proc. Natl. Acad. Sci.* **2010**, *107*, 8103.
[23] J. Gonzalo, C. N. Afonso, I. Madariaga, *J. Appl. Phys.* **1997**, *81*, 951.
[24] A. P. Chen, F. Khatkhatay, W. Zhang, C. Jacob, L. Jiao, H. Wang, *J. Appl. Phys.* **2013**, *114*, 124101.
[25] J. Gonzalo, R. Gómez San Román, J. Perrière, C. N. Afonso, R. Pérez Casero, *Appl. Phys. A: Mater. Sci. Process.* **1998**, *66*, 487.
[26] Y. J. Chang, S. H. Phark, *ACS Nano* **2016**, *10*, 5383.
[27] P. Yu, W. Luo, D. Yi, J. X. Zhang, M. D. Rossell, C.-H. Yang, L. You, G. Singh-Bhalla, S. Y. Yang, Q. He, Q. M. Ramasse, R. Erni, L. W. Martin, Y. H. Chu, S. T. Pantelides, S. J. Pennycook, R. Ramesh, *Proc. Natl. Acad. Sci. USA* **2012**, *109*, 9710.
[28] H. Yamada, A. Tsurumaki-Fukuchi, M. Kobayashi, T. Nagai, Y. Toyosaki, H. Kumigashira, A. Sawa, *Adv. Funct. Mater.* **2015**, *25*, 2708.
[29] A. M. Kolpak, D. Li, R. Shao, A. M. Rappe, D. A. Bonnell, *Phys. Rev. Lett.* **2008**, *101*, 36102.
[30] W. A. Saidi, J. M. P. Martirez, A. M. Rappe, *Nano Lett.* **2014**, *14*, 6711.
[31] J. Zuo, A. B. Shah, H. Kim, Y. Meng, W. Gao, J.-L. Rouviére, *Ultramicroscopy* **2014**, *136*, 50.
[32] B. Meyer, D. Vanderbilt, *Phys. Rev. B* **2001**, *63*, 205426.
[33] S. Jesse, A. P. Baddorf, S. V Kalinin, *Nanotechnology* **2006**, *17*, 1615.
[34] N. Balke, P. Maksymovych, S. Jesse, A. Herklotz, A. Tselev, C. Eom, I. I. Kravchenko, P. Yu, S. V Kalinin, *ACS Nano* **2015**, *9*, 6484.

© 2017 WILEY-VCH Verlag GmbH & Co. KGaA, Weinheim